Discovery of a Nasal Spray Steroid, Tixocortol, as an Inhibitor SARS-CoV-2 Main Protease and Viral Replication

Davis et al.

Supplemental Files

Fig. S1

A

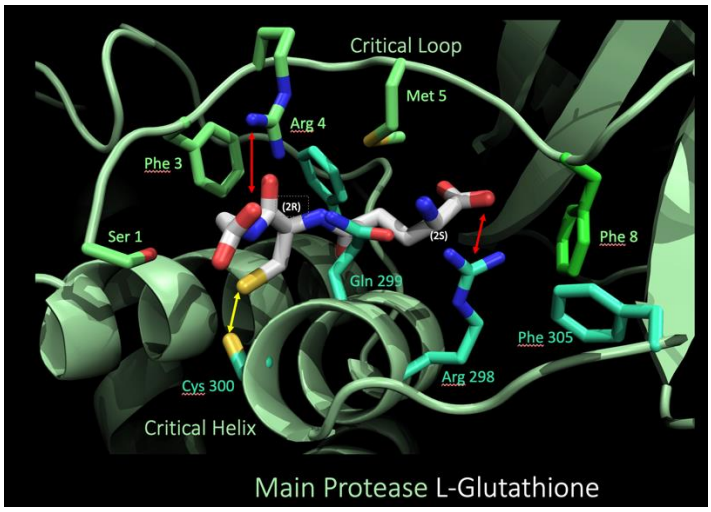

B

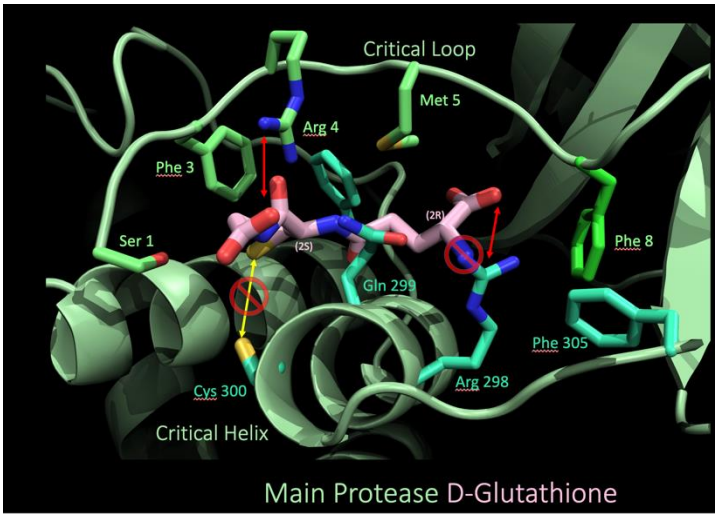

Fig. S1: Docking of L-glutathione and D-glutathione at the Cys300 pocket in SARS-CoV-2 M^{pro}. M^{pro} (showing one monomer of the dimer) is in green (PDB 7AXM) with (A) L-glutathione in stick model as red (oxygens), white (carbons), blue (nitrogens) or with (B) D-glutathione in pink (carbons), red (oxygens) and blue (nitrogens). The sulfhydryl groups are shown in yellow. Yellow arrows indicate potential disulfide bonds and red arrows indicate salt bridges for each glutathione form. In this model, L-glutathione forms favorable interactions from side chains on a critical loop and a critical helix. Once desolvated, the L-glutathione binding mode (A) is first dominated by salt bridge formations (Arg4 and Arg298). This places the 2S configuration of the L-glutathione sulfhydryl at a 2.54 angstrom distance from the Cys300 sulfhydryl, where a disulfide bond can easily form. By contrast (B), the D-glutathione 2S configuration of the sulfhydryl is too far away (5.48 angstroms) to form the Cys300-D-glutathione disulfide bond. The model also suggests that the 2R configuration of the amino group for D-glutathione forms unfavorable steric clashes if a salt bridge with the Arg 298 side chain were to form. See electronic supplemental information text for detailed description of model development†.

Table S1

		A	B	C
Compound	**Name**	**Dock Score**	**M^{pro} Activity (% control)**	**Covalent modification**
DB02025	Acv tripeptide	-4.769	159 +/- 7	no
DB00886	Omapatrilat	-4.504	99 +/- 11	no
DB08766	Zofenoprilat	-4.359	147 +/- 10	trace
DB03912	Phosphopantetheine	-4.34	163 +/- 13	non
DB08626	(S)-THIORPHAN	-4.302	134 +/- 10	no
DB01197	Captopril	-4.217	151 +/- 14	no
DB02032	Epicaptopril	-4.152	206 +/- 68	no
DB12160	bucillamine	-4.083	167 +/- 19	no
DB09091	**Tixocortol**	**-3.829**	**20 +/- 11**	**yes**
DB11164	Bicisate	-3.279	119 +/- 6	no
DB12192	Emeramide	-2.681	142 +/- 16	no
DB03760	(R)-dihydrolipoic acid	-1.06	95 + /- 14	no

Table S1: List of compounds identified based on docking prediction at Cys300 pocket in SARS-CoV-2 M^{pro} and their ability covalently modify M^{pro} and affect M^{pro} activity. Pipeline Pilot produced 72 compounds with -SH groups that could potentially dock at Cys300. To determine the feasibility of covalent binding, these thiol compounds were covalently docked into the SARS-CoV-2 M^{pro} crystal structure. Maestro 12.7 was used to prepare the template crystal structure 7MHI. We identified 15 compounds with docking scores favorable for the Cys300 pocket and 13 of these compounds were obtained for testing. **(A**) Docking scores obtained using Covalent Docking module to model the covalent ligand-protein complex using the reactive residue set at Cys300. Reaction Type of Disulfide Formation, and Docking Mode set at Virtual Screening. Note that glutathione's docking score (not shown) was -4.213. (**B**) M^{pro} activity was measured using a peptide based HPLC assay using 100 nM M^{pro} and 50 µM of each drug (see supplemental slide 1). Drugs were incubated for 1-hr then the assay was started with addition of peptide substrate and stopped after 10 minutes. Products were determined by measuring their absorbance at 205. Control was 5% DMSO and all samples contained 5% DMSO in assay. Note that only tixocortol showed significant inhibitory activity against M^{pro} while most others showed increased activity. (**C**) Each compound (50 µM) was incubated with M^{pro} (5 µM) for 1 hr in assay buffer and then analyzed by SEC/MS to assess covalent modification based on the amu for M^{pro} species.

Fig. S2

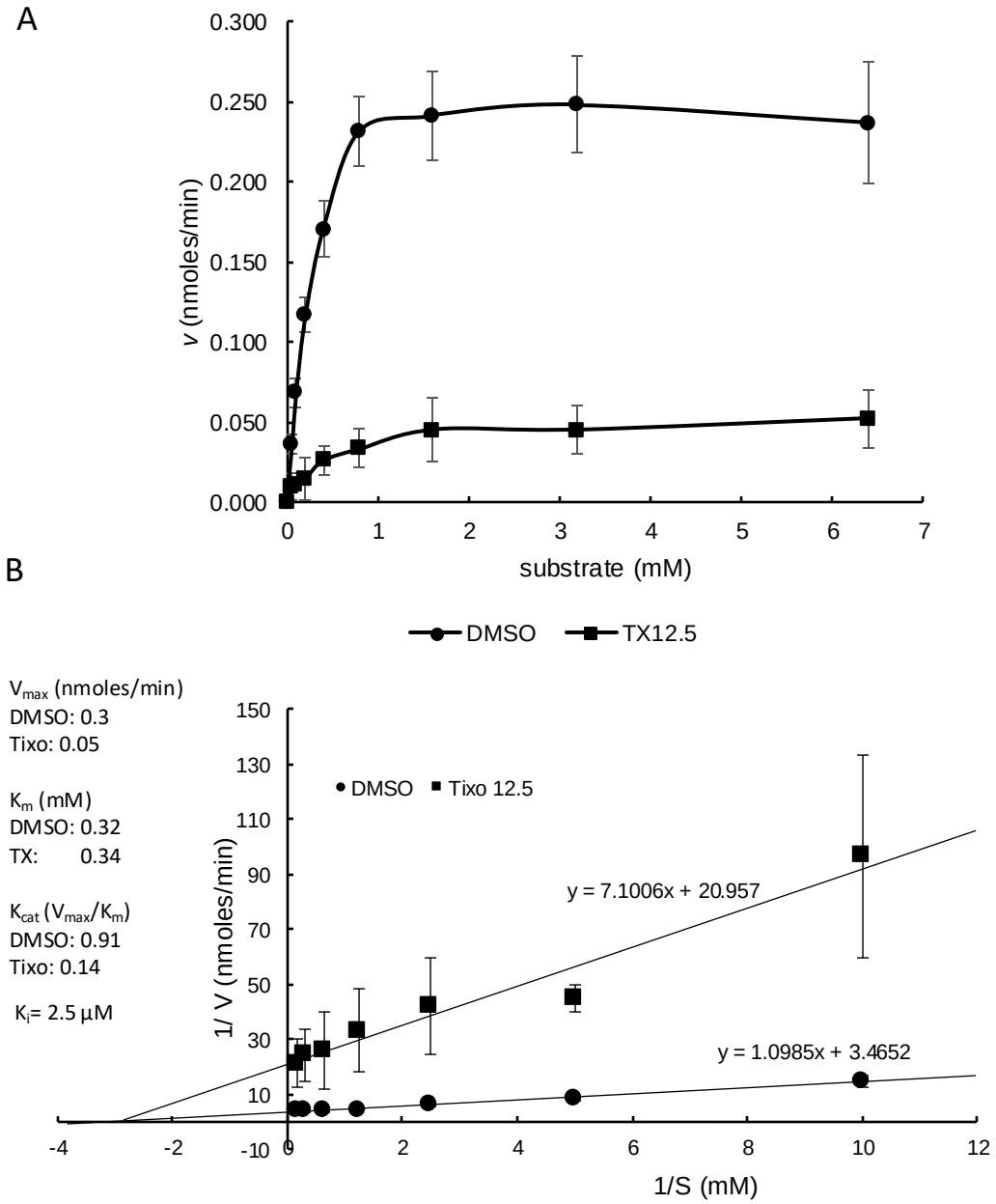

Fig. S2: Michaelis Menten Kinetic analysis of WT SARS-CoV-2 M^{pro} activity in the absence and presence of tixocortol. Authentic WT M^{pro} was preincubated in 50 mM HEPES buffer pH 7.8, 1 mM EDTA, 250 ug/ml BSA and 50 mM NaCl and treated with DMSO (5%) or tixocortol (12.5µM in final 5% DMSO). After 1 hr, peptide was added and the assay (50 nM M^{pro}) carried out for 8 min in the linear region for this assay. The concentration of the peptide substrate was varied from 0.05 to 6.4 mM to determine the initial velocity for M^{pro}. (A) The Michaelis Menten plot is substrate vs initial rate (v) in nanomoles of product per minute. Average and standard deviation was calculated from the data from three separate experiments (2 experimental values for the 0.8 mM substrate in DMSO treated) and are presented as the mean ± standard deviation (SD). (B) Lineweaver-Burk plot for tixocortol-induced SARS-CoV-2 WT M^{pro} inhibition, control (circles), 12.5 µM tixocortol (squares). The error bars represent the standard deviation from three independent experiments. The data indicates non-competitive inhibition (similar K_m values with decreased V_{max}). The error bars represent the standard deviation (note that only two data points plotted for 0.2 mM [S)]. The data indicates non-competitive inhibition with a calculated apparent K_i of 2.5 µM under these conditions.

Fig. S3

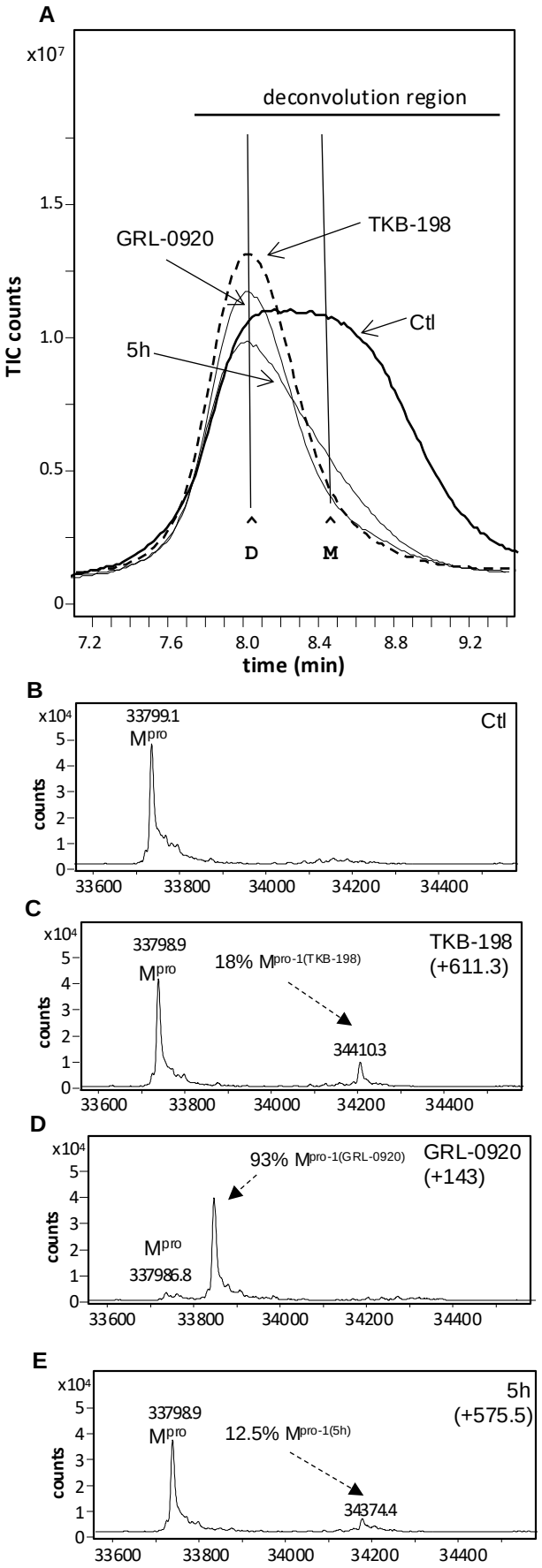

Fig. S3: SEC analysis of the oligomeric state of M^{pro} and assessment of covalent modification by MS following treatment with GRL-0920, TKB-198, 5h . M^{pro} (10 µM) was incubated at 37^{0}C with DMSO control, TKB-198, GRL-0920 or 5h (200 µM) (in 50 mM HEPES buffer pH 7.8 and 1 mM EDTA in a final of 15% DMSO for 1 hr and then analyzed by SEC-MS. (A) Elution profile for Mpro control and drug treated samples. Shown in the left panels (B, C, D, and E) is the determination of covalent modification of M^{pro} following protein deconvolution of the TIC for the eluting M^{pro} species for (B) control, (C) TKB-198, (D) GRL-0920 and (E) 5h. TIC for each condition.

Fig. S4

A

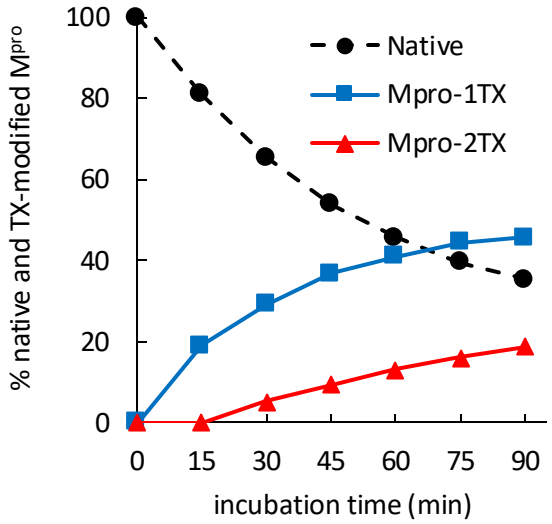

B

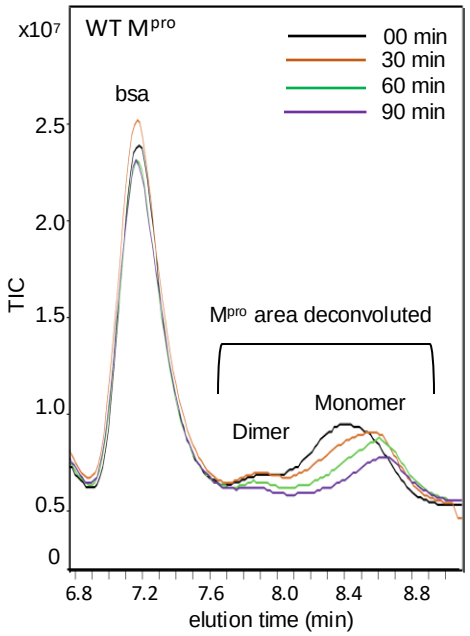

C

M^{pro} mass 33797 da	M^{pro}-1TX mass 34174	M^{pro}-2TX mass 34550	Ion species extracted
1252.74	1266.67	1300.83	27^+
1300.83	1315.33	1329.75	26^+
1352.84	1367.9	1382.97	25^+
1409.16	1424.85	1440.56	24^+
1470.39	1486.76	1503.13	23^+
1537.18	1554.28	1571.42	22^+
1610.33	1628.26	1646.20	21^+
1690.79	1709.62	1728.51	20^+
1779.72	1799.55	1819.3	19^+
1878.5	1899.46	1920.43	18^+

D

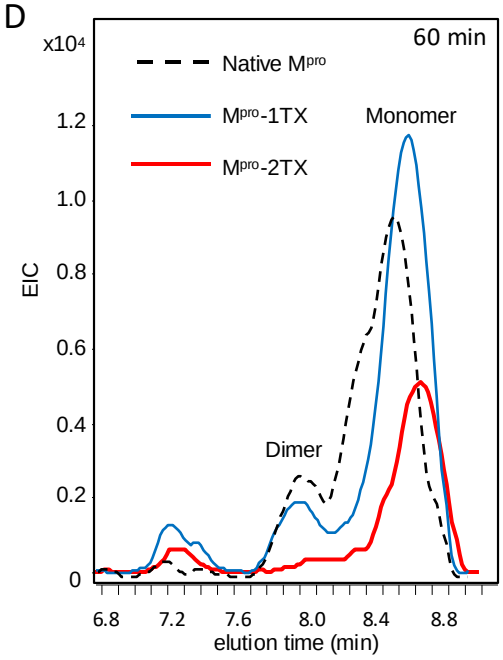

Fig. S4: Covalent modification of SARS-CoV-2 WT M^{pro} by tixocortol over a 90-minute period. WT M^{pro} at 1 µM was incubated with 200 µM TX in 50 mM HEPES buffer pH 7.8 with 50 mM NaCl and 1 mM EDTA and incubated at 37^0C and then analyzed by SEC-MS. Carboxy methylated BSA (250 ug/ml) was included as an internal control. (A) Percent of native and TX modified forms of M^{pro} (Mpro-1TX and Mpro-2TX) obtained over time by protein deconvolution of the eluting M^{pro} shown in (B) SEC/MS chromatography for eluting M^{pro} treated with TX from 0- 90 min. (C) Molecular weights for native M^{pro} and TX modified M^{pro}'s and their associated prominent molecular ion species generated by mass spectrometry prior to deconvolution. (D) Elution profile obtained for each M^{pro} species after 60 min of TX treatment. Each elution profile was obtained by using extracted ion current (from 6.8-9 min) for the ions specific to each M^{pro} species. Native M^{pro} (**black** hashed tracing), M^{pro}-1TX (blue tracing) and M^{pro}-2TX (red tracing). The ions associated with each species as seen in the table were extracted to reveal the elution profiles for the different M^{pro} species following size exclusion chromatography as seen in Figure S4B.

Fig. S5

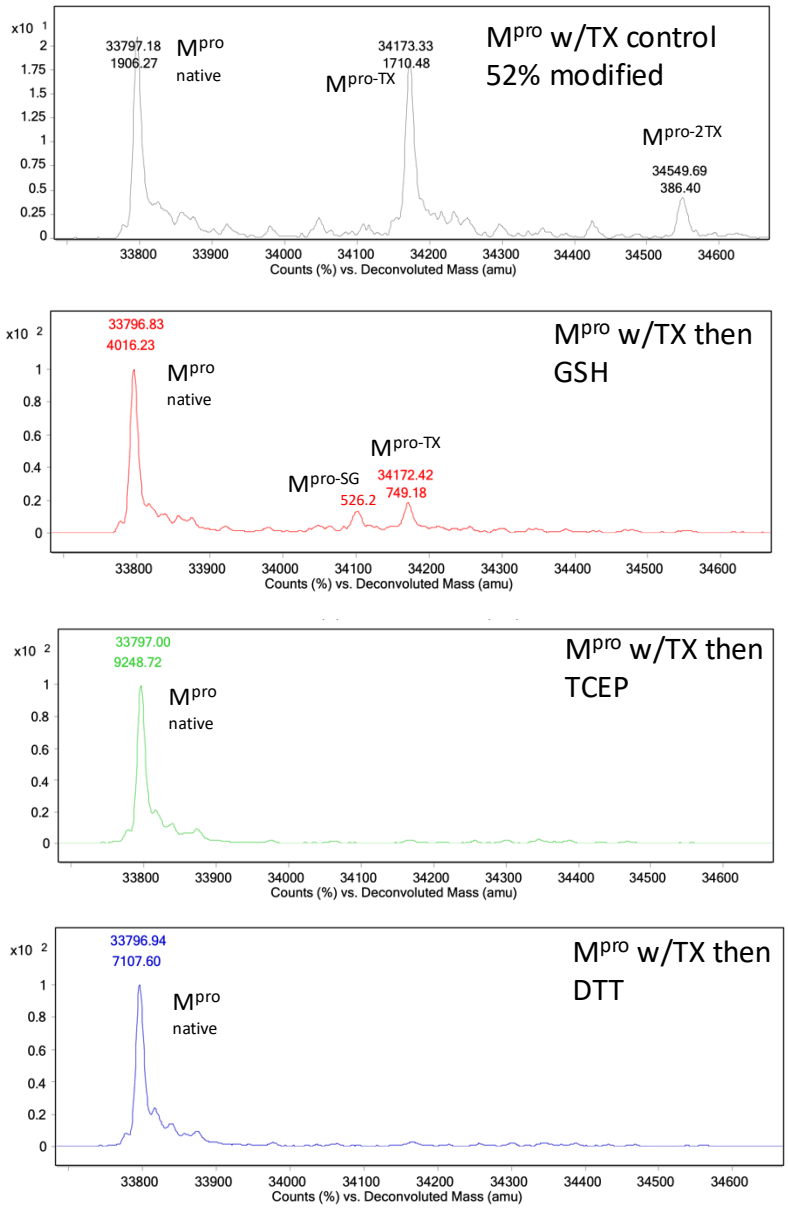

Fig. S5: Reversal of TX-modification of M^{pro} with different reducing agents. M^{pro} (1 µM) was incubated with 50 µM TX in assay buffer for 1 hr then reducing agents were added (diluted 1:20 as 20X stocks) to give a final concentration of 10 mM for 15 minutes. (water was used as a control) and samples then assayed by SEC/MS. Shown is the deconvolution for M^{pro} for water control, GSH (20 mM), TCEP, or DTT 10 mM for 15 min.

Fig. S6

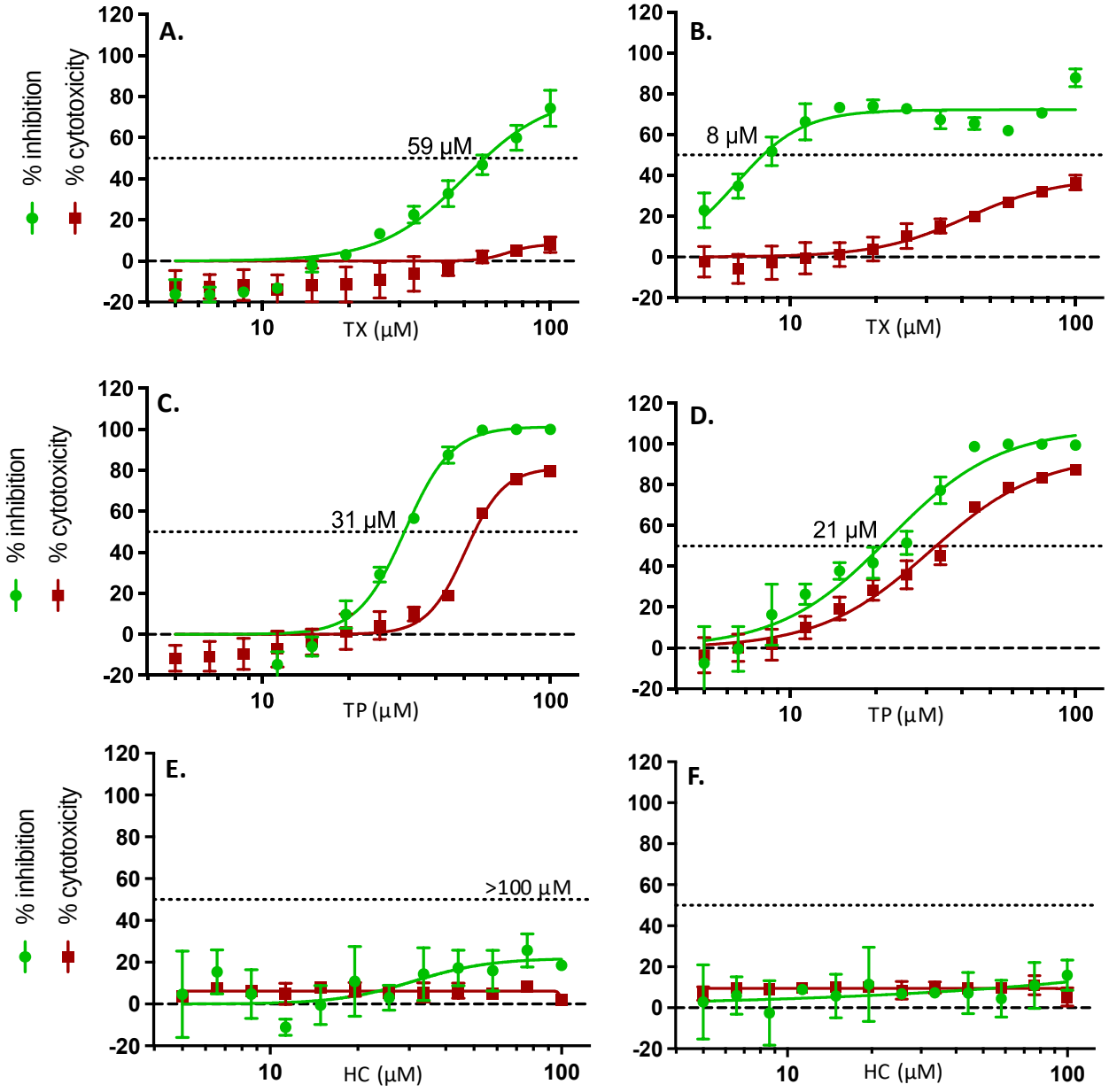

Fig. S6: Inhibition of SARS-CoV-2 replication in HeLa -ACE2 cells following a 1-hr or 18-hr pretreatment with TX, TP or HC. High-content imaging assays were performed to determine compound potency (green line), and CellTiter-Glo assays were performed to determine cell viability (red line). HeLa cells were grown in typical heat-inactivated serum. Cells were pretreated with drugs (TX,TP, or HC) for 1 hr (A, C and E) or 18 hr (B, D and F) prior to exposure to SARS-CoV-2. Results are reported as percentage inhibition of virus replication (green values) and cytotoxicity (red values) relative to untreated controls. Error bars represent standard deviations (SDs) from tests run for each concentration with 4 replicates. IC_{50}, half-maximal inhibitory concentration is indicated for each drug on the dotted line.

Fig. S7

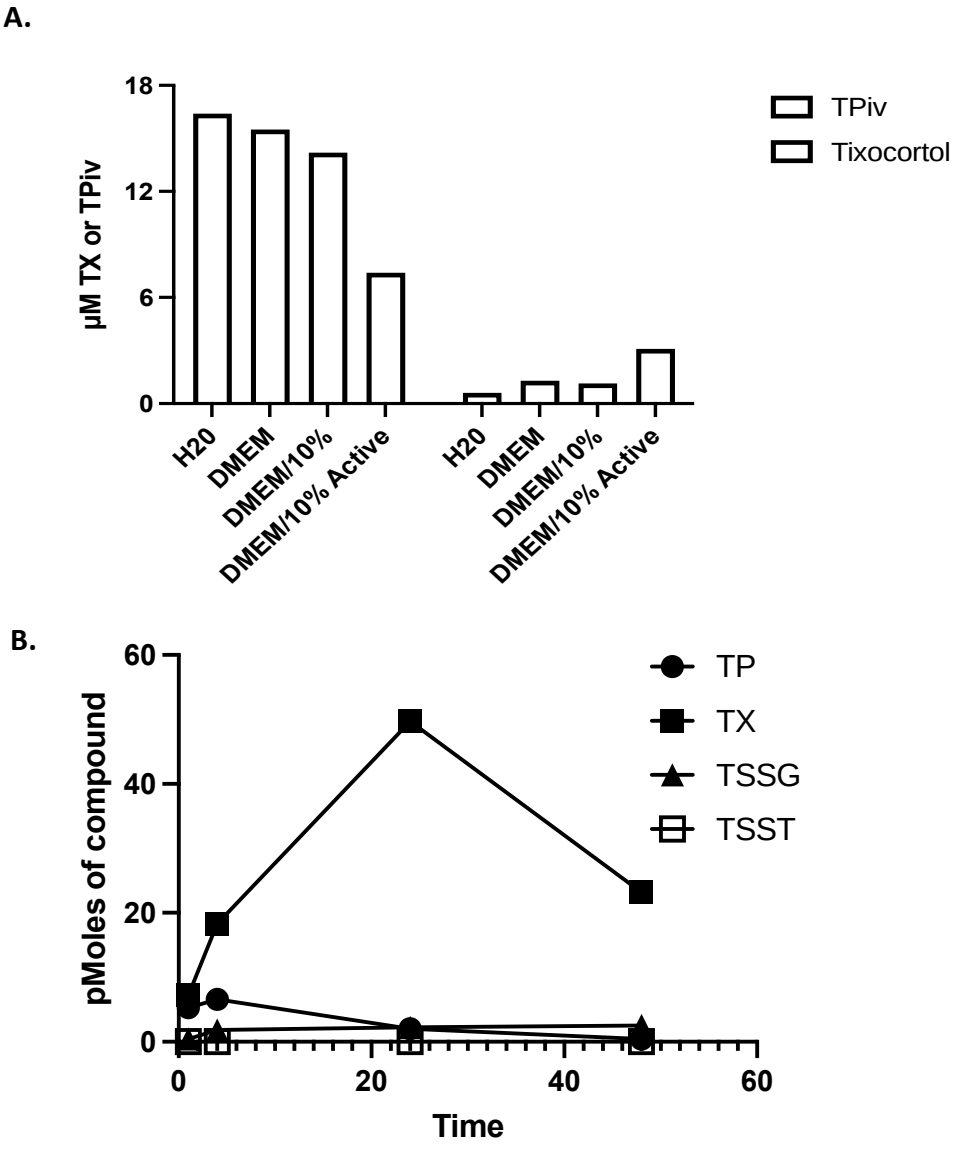

Fig. S7: Metabolic fate of TP added to HeLa cells. (A) TP (25 µM final) was incubated in H2O, DMEM, DMEM with 10% heat inactivated serum, or DMEM with 10% serum not heat inactivated. Samples were left overnight (18 h) at 37^0C. Samples were then diluted with DMSO (50% final), acidified with TFA (0.1%) and treated with TCEP (10 mM) to recover any disulfide bound TX released from TP. The amount of TP and TX recovered from the samples was determined based on TP and TX standards. (B) HeLa cells were plated overnight and then cells were treated with TP (50 µM). Cells were then extracted for metabolites after 1, 4, 24, and 48 hr incubation. Cells were washed with PBS the cells were then trypsinized followed by three washes with PBS. The pellet was then extracted with 60% methanol solution/0.2% TFA and heated at 95 degrees for 5 minutes. Cellular debris was removed by centrifugation and the methanolic/TFA solution dried by speed vac to dryness. The residue was dissolved in 100% DMSO and analyzed by RP-HPLC/MS. Shown are the levels of TP, TX, TSSG and the disulfide of TX.

Fig. S8

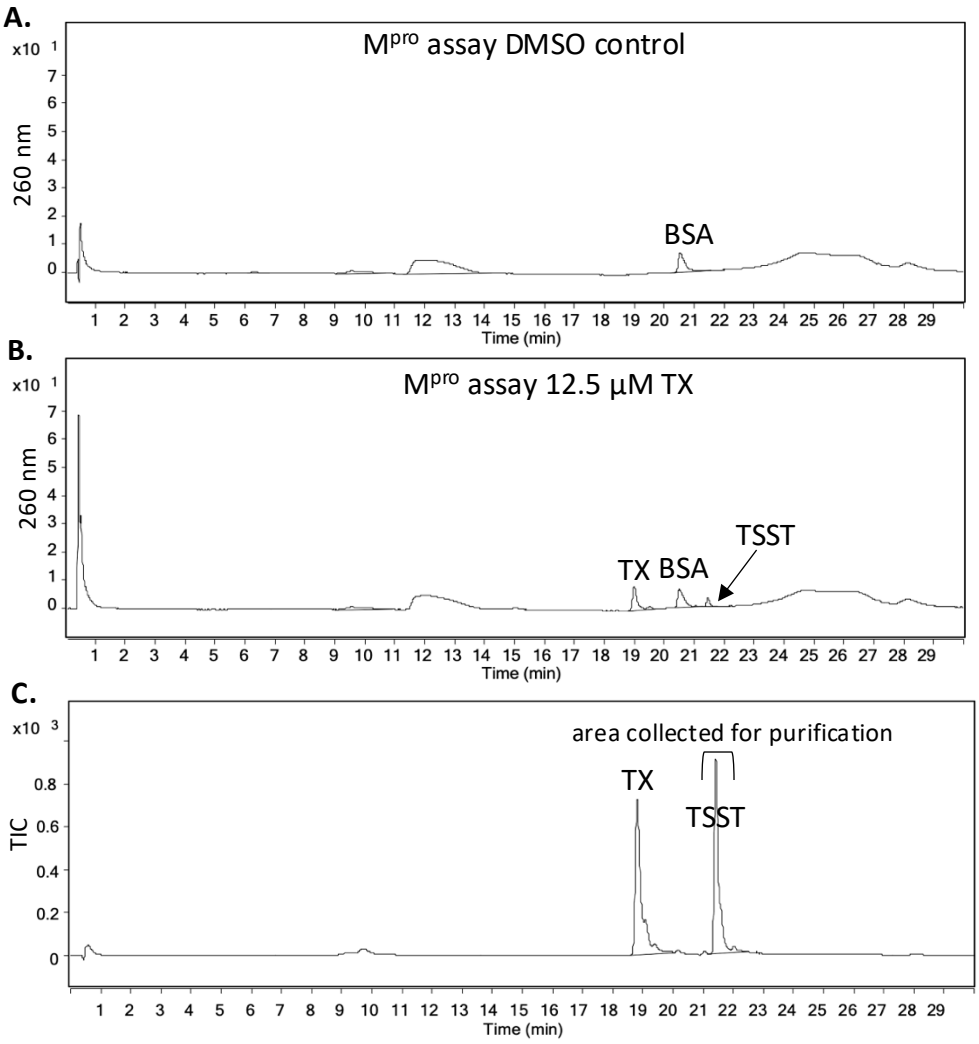

Fig. S8: Identification of the production of TSST in M^{pro} assays with TX and purification of TSST. The peptide assay was done as described for MM kinetics. A) DMSO treated control M^{pro} (50 nM) with 1.6 mM substrate analyzed at 260 nm to detect the steroid ring. B) TX treated (12.5µM) M^{pro} (50 nM) with 1.6 mM substrate. Shown above UV tracing at 260 nm that reveals TX, TSST due the typical absorption for α, β-unsaturated ketones and BSA and . C) TX and TSST were identified by mass spectrometric analysis following the RP-HPLC C18 chromatography shown is the TIC chromatogram. For purification of TSST, TX (1 mM) was incubated overnight in HEPES buffer pH 7.8 and 10% DMSO. A precipitate formed which contained the majority of TX and TSST. This was redissolved in 100% DMSO and then run on RP-HPLC (assay method) to separate TX from TSST. The area for the eluting TSST was collected as shown above using the assay RP-HPLC method.

Fig. S9

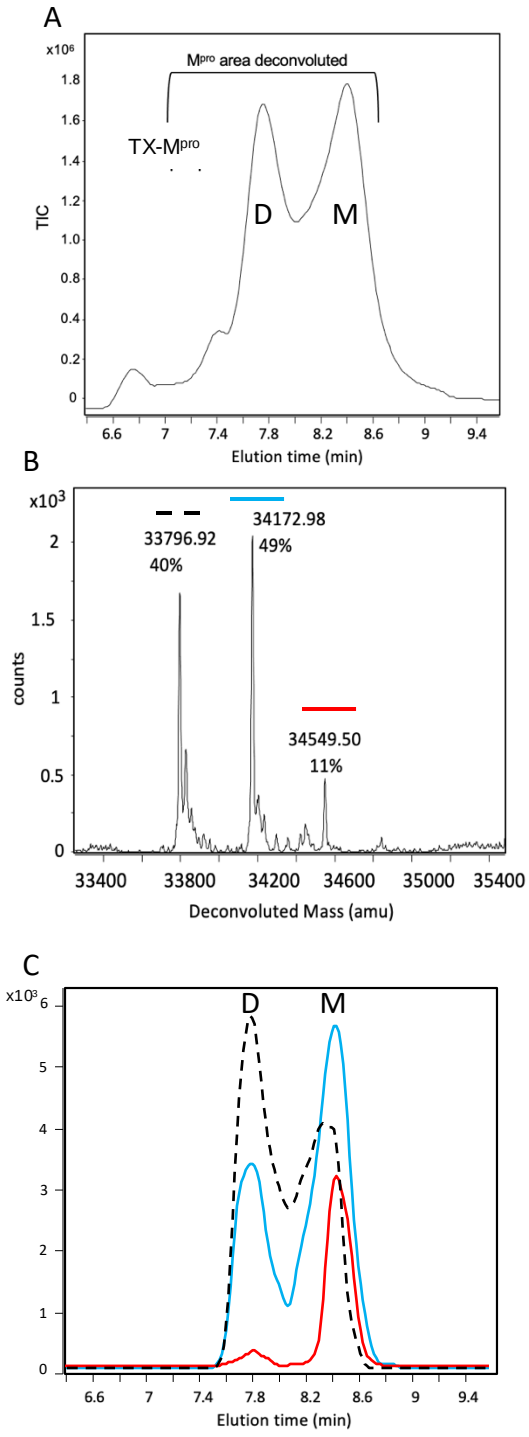

Fig. S9: SEC analysis of the oligomeric state of TX-M^{pro} and assessment of covalent modification by MS protein deconvolution. TX-M^{pro} was prepared as described in materials and methods and then analyzed by SEC/MS. (A) SEC behavior of TX-M^{pro} revealing both dimer and monomer peaks for M^{pro} as indicated. (B) Protein deconvolution of TX-M^{pro} showing percent native and TX-modified forms of M^{pro}. (C) Elution profile obtained for each M^{pro} species in the TX-M^{pro} preparation using extracted ion current (from 6.5-9.5 min) for the ions specific to each M^{pro} species (see supplemental file 2 for extracted ions). Native M^{pro} (black hashed tracing), TX1-M^{pro} (blue tracing) and 2TX-M^{pro} (red tracing).

Fig. S10

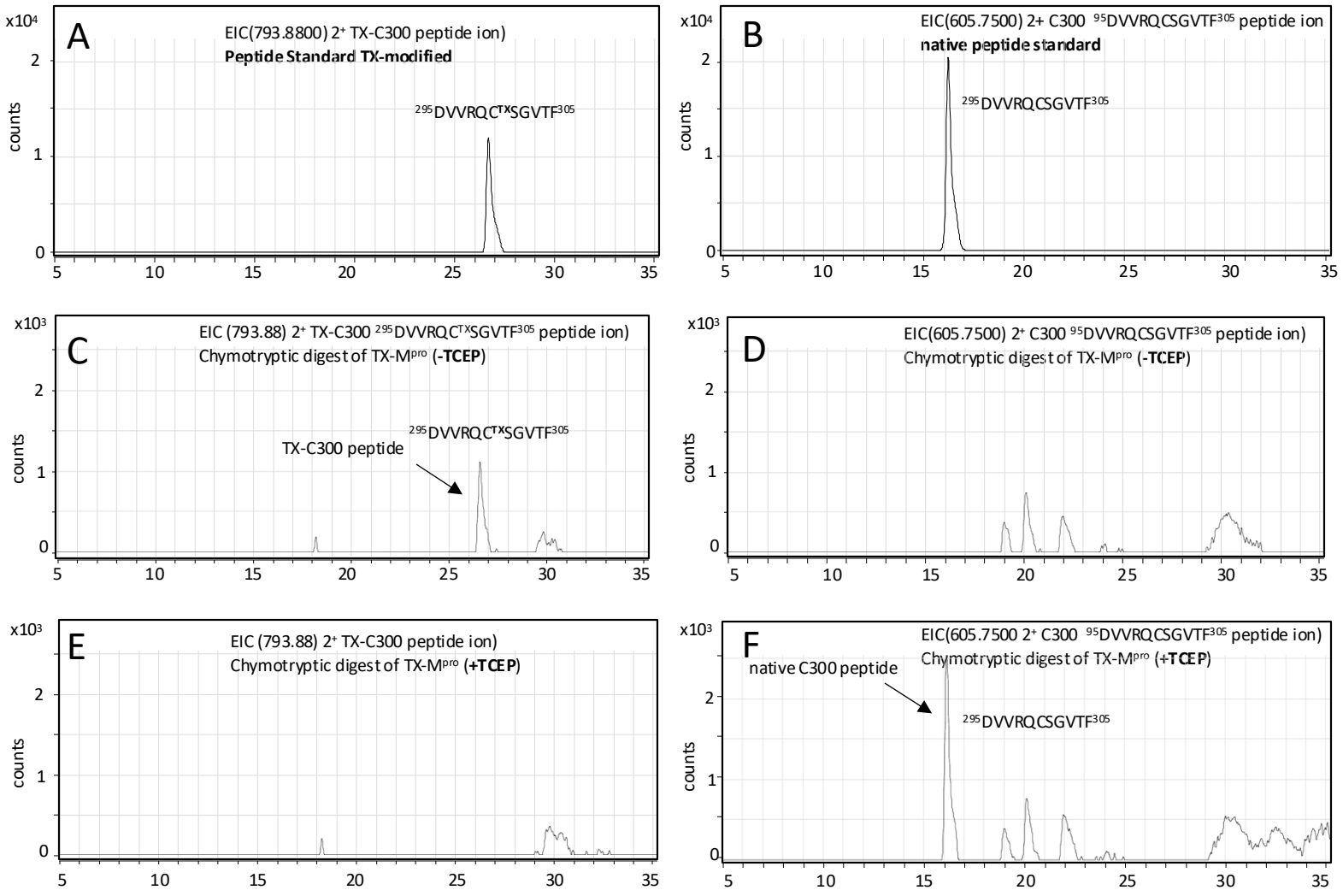

Fig. S10: Identification of TX modification of Cys300 in chymotryptic digests of the TX-M^{pro} preparation. The TX-M^{pro} preparation was alkylated and digested with chymotrypsin as described in the materials and methods and then analyzed by RP-HPLC/MALDI-TOF for the identification of M^{pro} chymotryptic peptides. (A,B) Elution profile for (A) the TX-Cys300 ^{295}DVVRQC^{TX}SGVTF^{305} peptide standard or (B) the corresponding ^{295}DVVRQCSGVTF^{305} native peptide standard. (C,D) Identification of (C) TX-modified Cys300 peptide in the chymotryptic digests of TX-Mpro and (D) absence of detection of the native Cys300 peptide prior to TCEP treatment. (E,F) Loss of detection of (E) detection (F) of the native Cys300 peptide following TCEP treatment of the peptide digest. peaks were identified by ion extraction of the 2$^+$ forms of the Cys300 peptide as indicated.

Fig. S11

Cys Number	Peptide Sequence/mass	Calculated monoisotopic mass after alkylation	Peptide ions observed	RT (min)	% TX modified Peptide estimated
16	PSGKVEG**C**M (906.4)	1031.4	516.7^{2+}	20.1	0
22	VQVT**C**GTTL (920.5)	1045.5	523.7^{2+}	13.7	0
38,44	**C**PRHVI**C**TSEDMLNPNY (1990.9)	2240.9	NF	-	-
85	RVIGHSMQN**C**VL (1355.7)	1480.7	741.3^{2+}	20.2	0
117	SVLA**C**Y (654.3)	779.3	780.4^{1+}	17.0	0
128	Q**C**AMRPNF (965.4)	1090.5	546.3^{2+},1091.5^{1+}	19.8	0
128*	pyQ**C**AMRPNF (948.4)	1073.5	537.8^{2+}	20.6	0
145	LNGS**C**GSVGF (939.4)	1064.4	533.2^{2+} ,1065.4^{1+}	15.0	0
145**	TIKGSFLNGS**C**GSVGF (1572.8)	1697.8	849.9^{2+}	16.9	0
156	D**C**VSF (569.2)	694.2	695.2^{1+}	9.7	0
156***	NIDYD**C**VSF (1209.6)	1199.4	600.7^{1+}	22.0	0
160	CY (284.1)	409.08	NF	-	-
265	DM**C**ASLKEL (1008.5)	1133.5	567.8^{2+}	19.7	0
300	DVVRQ**C**SGVTF (1209.6)	1334.6	668.3^{2+}	19.0	25
300****	DVVRQ**C**SGVTFQ (1337.6)	1462.6	732.3^{2+}	17.4	37

Fig. S11: Cysteine containing peptides identified after chymotrypsin digestion. Shown is the amino acid sequence for each Cys containing peptide, the monoisotopic mass for the native and alkylated forms and the peptide ions observed for each peptide. * This peptide containing cysteine 128 occurs (about 50% is this form) due to spontaneous deamidation which is known to occur with N-terminal glutamine residues. ** This peptide containing Cys145 results from incomplete cleavage at the 140:141 predicated chymotryptic cleavage site.***This peptide containing cysteine 156 results from incomplete cleavage at the 154:155 predicted chymotryptic cleavage site. ****This peptide containing Cys300 occurs as a result of incomplete cleavage at the 305:306 predicted chymotryptic cleavage site. NF=Not found.

Fig. S12

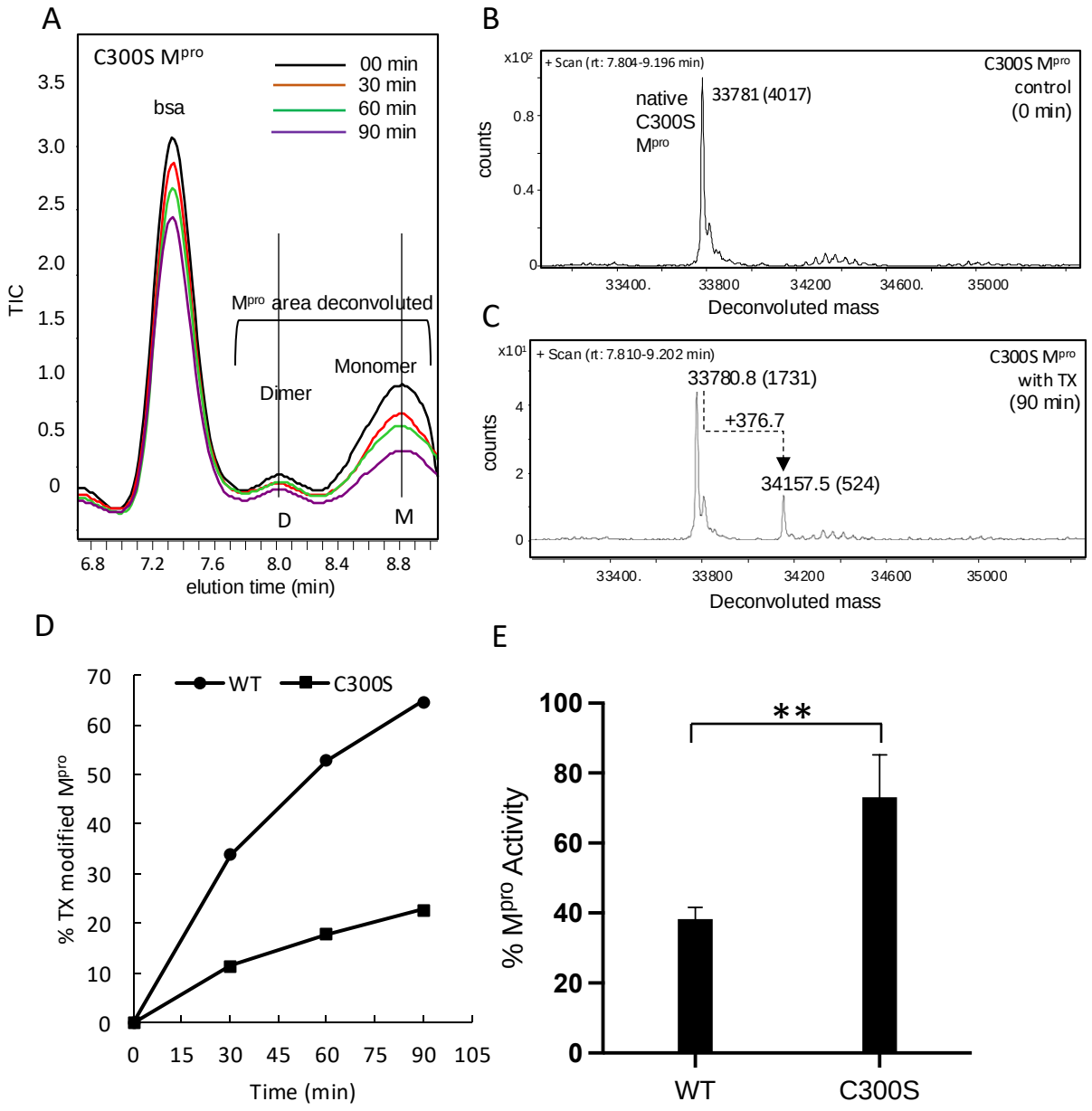

Fig. S12: SEC/MS analysis of the oligomeric state and covalent modification of SARS-CoV-2 C300S M^{pro} treated with TX over a 90 minute period. (A) Elution profile for C300S M^{pro} treated with TX (200:1 ratio) at 0, 30, 60 and 90 minutes after TX treatment. C300S M^{pro} at 1 µM was incubated with 200 µM TX in 50 mM HEPES buffer pH 7.8 with 50 mM NaCl and 1 mM EDTA and incubated at 35^{0}C and then analyzed by SEC-MS. BSA (250 ug/ml) was included as an internal control. Total ion current was used to detect the eluting protein. (B,C) Protein deconvolution of C300S M^{pro} eluting between 7.8 and 9.2 min at (B) time 0 and (C) 90 minutes after incubation with TX (200:1) showing the masses observed consistent with a single TX modification of C300S M^{pro}. (D) Shown is the percent TX modified M^{pro} for WT M^{pro}(circles) and C300S M^{pro} (squares) at different time points after TX treatment. (E) M^{pro} activity was measured using the peptide based HPLC assay with 50 nM of each M^{pro} and 12.5 µM of TX. M^{pro}'s were incubated for 1-hr then assayed for 10 minutes. Products were determined by measuring their absorbance at 205nm. WT and C300S values represents 3 independent experiments, error bars are +/- SD, students T-test *P<0.01.

Fig. S13

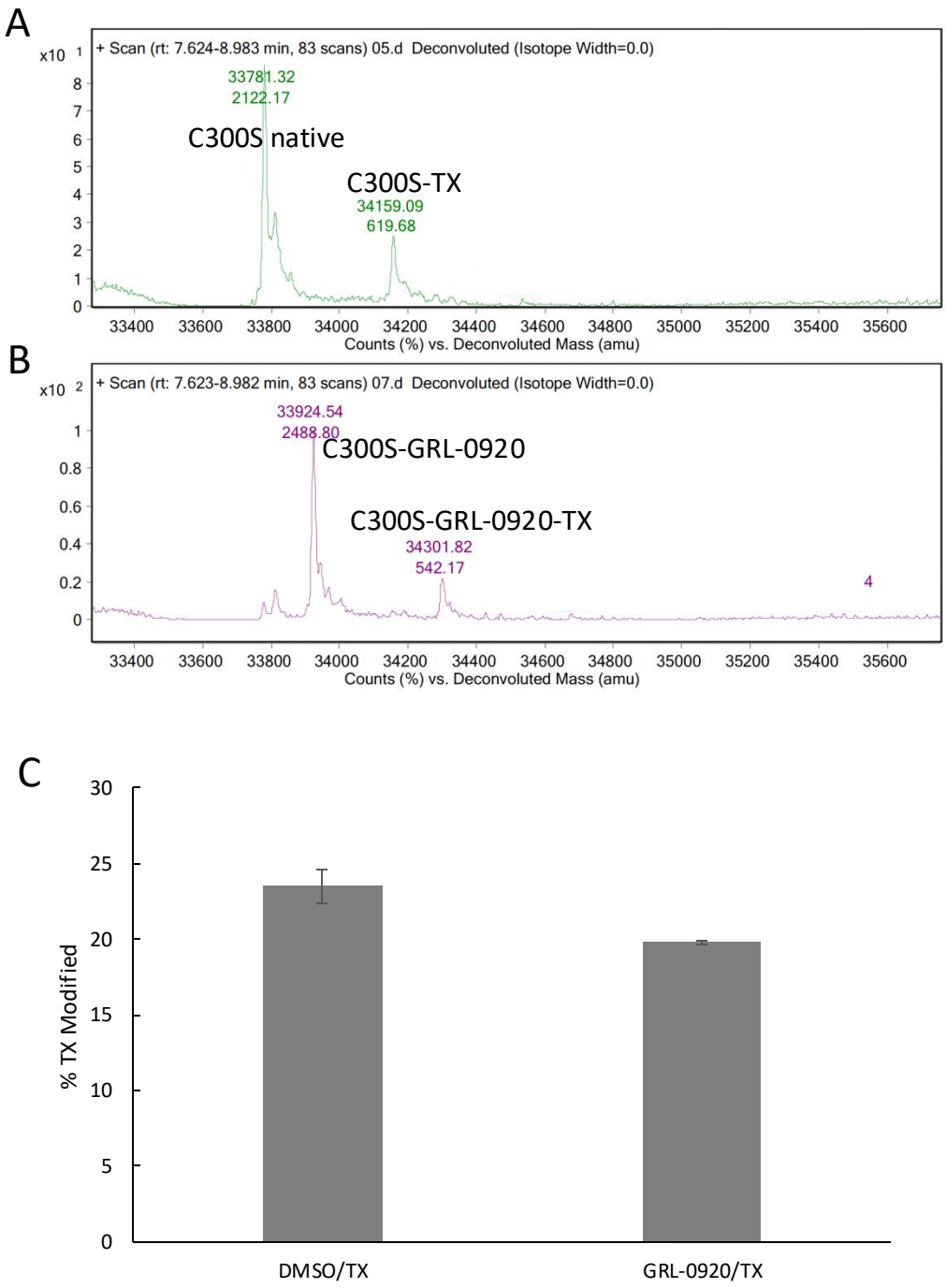

Fig. S13: Assessment of TX covalent modification of C300S without or with GRL-0920 pretreatment to covalently occupy the active site cysteine. Deconvolution following SEC analysis of (A) C300S M^{pro} treated with TX (200:1) for 30 min or (B)) C300S M^{pro} pretreated with GRL-0920.The masses for the TX modified and GRL-0920 modified proteases are indicated.(C) Quantification of TX modifed C300S Mpro without or with pretreamtent with GRL-020 to occupy Cys145. The results are an average of 3 experiments with one example shown in A and B.

Fig. S14

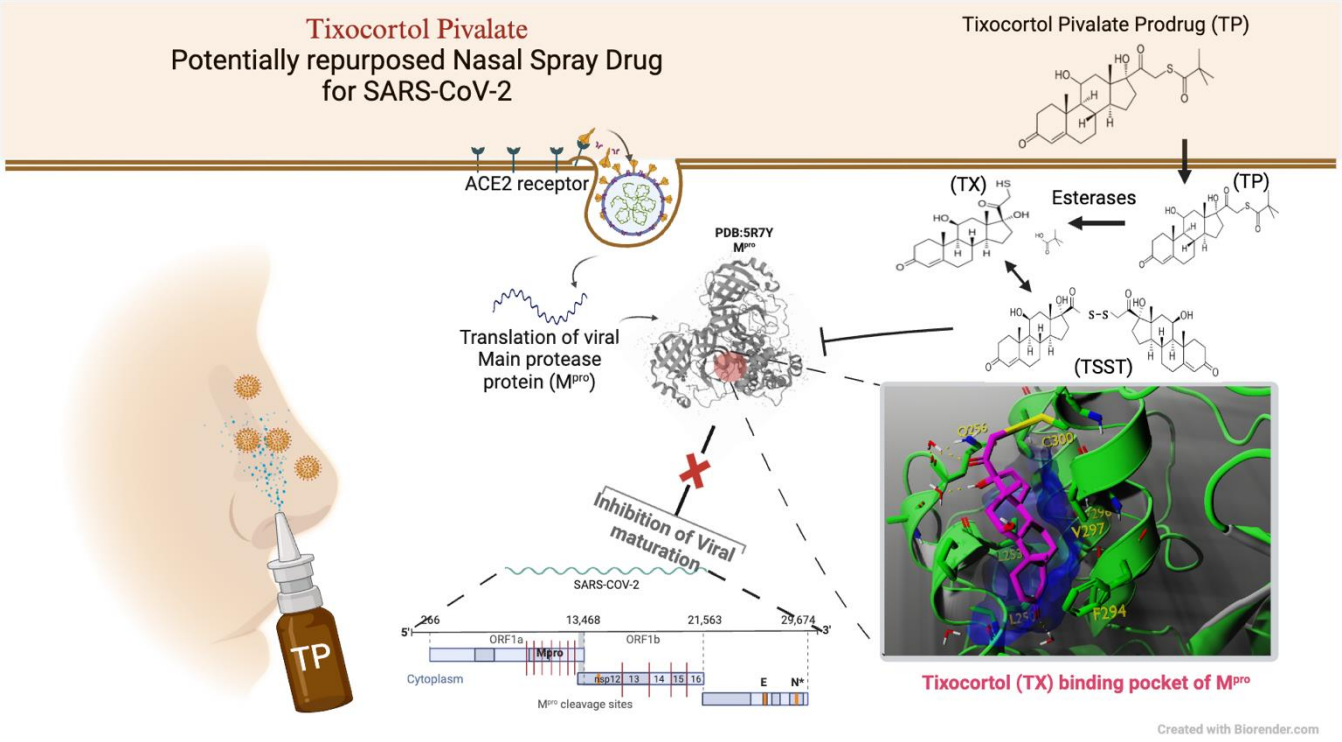

Fig. S14: Proposed schematic depicting the action of tixocortol pivalate against M^{pro} and SARS-CoV-2 replication. TP undergoes conversion to TX by serum and cellular esterases. In cells, TX may undergo further conversion to TSST, however both TX and TSST can covalently modify and inhibit M^{pro} activity thereby preventing the replication of SARS-CoV-2.

† *Electronic Supplementary Information*

Discovery of a Nasal Spray Steroid, Tixocortol, as an Inhibitor SARS-CoV-2 Main Protease and Viral Replication

David A. Davis[a], Ashwin Nair[a], Yana Astter[a], Emma Treco[a], Brian D. Peyser[b], Rick Gussio[E], Tam Luong Nguyen[b], Haydar Bulut[a], Brett Eaton[c], Michael Murphy[c], Prabha Shrestha[a], Shin-Ichiro Hattorri[d], Hiroaki Mitsuya[a,d] and Robert Yarchoan[a]

a. *HIV and AIDS Malignancy Branch, Center for Cancer Research, National Cancer Institute, Bethesda MD*
b. *Developmental Therapeutics Program, Division of Cancer Treatment and Diagnosis, National Cancer Institute, National Institutes of Health*
c. *Integrated Research Facility at Fort Detrick, 8200 Research Plaza, Frederick, MD 21702*
d. *National Center for Global Health and Medicine Research Institute, Department of Refractory Viral Infections, 1-21-1 Toyama Shinjuku-ku, Tokyo 162-8655, Japan*
e. *Vaccine Branch, Center for Cancer Research, National Cancer Institute, Frederick National Laboratory for Cancer Research, Frederick, MD 21702*

Molecular docking of glutathione and compound discovery procedure:

The objective was to form an all-atom detailed molecular model around L-glutathione. Among the SARS-CoV-2 main protease structures examined from the Protein Data Bank, there are marked similarities in their secondary and tertiary features. For the preliminary model, we chose the M^{pro} X-ray structure PDB:7AXM (1), the monomeric main protease that has been co-crystalized with Pelitinib. In this initial phase, the preliminary model served as a basis for ligand discovery.

Creation of the Preliminary Model

Structural alignments and structural sequence comparisons were performed with the Schrödinger Maestro V12.0.012, or Biovia's Discovery Studio V18.1. Protein preparation (potential assignment, preliminary optimization) was performed with both versions as well. Discovery Studio was employed to transfer potentials into compatible radii into the Biosym Discovery package. With respect to the development of a Main protease/ L-Glutathione_2S_2R model, we compared the ability of L-glutathione and D-glutathione to interact with a modelled subsite adjacent to the C300 of the main protease of SARS-CoV-2. Pelitinib was removed from the model. Detailed molecular docking studies were conducted to explore conformational space near a loop at the top of the helix containing C300. The objectives and requirements were:

1) Create a preliminary model where protein/atom-ligand/atom contacts show biochemical feasibility and chemical complementarity between glutathione and the protein binding site. The side chains of hydrophobic protein residues will form hydropathic favorable interactions (hydrophobic-hydrophobic, hydrogen bonding, acid-base) with complementary atoms of glutathione. More importantly, polar residues and backbone atoms of the protein are not allowed to form unfavorable hydropathic contacts (hydrophobic-polar, acid-acid, base-base) with the

main protease. When needed, hydropathics could be evaluated using the HINT software (4), or when small molecule parameters are missing, atom types and distances can be found in other high resolution X-ray structures as a model for the hydropathic non-bonded interactions.

2) Since the putative binding site is shallow, both glutathione enantiomers must be partially buried from the solvent-protein interface (Stern layer). Since L-Glutathione has confirmed activity, it will serve as a template for the binding model of D-Glutathione, since both have isomeric structures. The starting conformation for docking is assumed to initiate from the oxidation of L-Glutathione S-H and the C300 S-H.

3) Sterically, van der Waals violations can be no greater than 0.5 angstroms (bump violations). This would enable molecular mechanics optimizations (energy refinement) to proceed directly. Importantly, these docking objectives were performed with all-atom models (fully hydrogenated). An all-atom model would be equivalent to an X-ray structure having a resolution of 0.5 angstroms (0.6 angstrom resolution is the limit for X-ray diffraction).

4) Both carboxylate residues of glutathione must be balanced electrostatically (neutral charge) with complementary cationic side chains (e.g., Lys or Arg), or counterions (e.g., Na+ or K+). In the main protease sequences, Lys and Arg are often interchangeable.

5) Wherever possible, hydrogen bonds will be formed either directly between the appropriate ligand polar atoms and protein side chains or backbone atoms, or indirectly via water bridges.

6) The anchor for the interaction is the C300 side chain which must maintain a disulfide bond with the L-glutathione S-H.

7) The overall objective is to create an accurate model that can be used for ligand discovery or ligand design. As more data becomes available, and these data conflict with the structure activity relationship (SAR) inherent to protein/ligand contacts, the models will be improved or rebuilt.

Thus, detailed models are considered only a work-in-progress, until 100% of the structure activity relationships are explained.

Using the disulfide bond as the starting point for the docking, all rotatable bonds (10 for each glutathione) were systematically explored until the preliminary modeling objectives (see above) were achieved. Amide bonds were explored in their trans conformations, unless trans conformational isomers prohibited biochemical feasibility during the evolution of the model. This was never the case in this study. During molecular docking, if steric clashes were observed, the surrounding loop residues of protein were moved so that space would allow the glutathione to partially bury the compound out of the first hydration layer. In an iterative manner, both protein and ligands were checked for intramolecular bump and hydropathic violations and remodeled until these were eliminated. The preliminary model was developed using the Biovia Insight II (2005) molecular modeling suite with full SGI dialbox capability. Ligand construction and conformational exploration (molecular mechanics dynamics and optimizations) was performed using the ChemOffice 3D package utilizing MM2 and MM4 force field parameters.

Preliminary Model Energetic Refinement

Molecular mechanics simulations consisted of combining steepest descents with conjugate gradient optimizations (Fletcher Powel optimization) utilizing the cff91 class II force field from the Discover molecular mechanics package. First the sterically and hydropathically feasible model was built according to the criteria above. Next, the ligand was fixed to enable residues of the main protease to adjust their side chain disposition about the ligand conformation that was developed during preliminary modeling phase. Once hydrogen atoms were optimized, the backbone atoms remained fixed so that the side chains were allowed to optimize first. If the model lacked bump violations (< 0.25 angstrom Van Der Waal overlap) the entire residues between Ser A1 to Phe A8 were then allowed to relax, while the backbone

remained tethered using constraints up to 100 Kcal/angstrom^2. Optimization proceeded until the norm of the gradient was less than 0.5 Kcal/angstrom. At all times, a harmonic constraint between the L-glutathione S and the γ-S of the C300 residue was enforced with 20 Kcal/angstrom force at the lower boundary, and a 100 Kcal/angstrom at the upper limit. We found it necessary to add an additional constraint between the α-C of the Val A296 residue and the O4 of the ligand to prevent the formation of a hydrophobic unfavorable interaction during minimization. In this case, a lower limit of 3.65 Å was enforced between any polar atom/hydrophobic pair with Val A296 and O4 of L-glutathione (the hydropathic minimum distance for carbon polar atom contacts). A 4.0 Å upper limit was employed for this constraint as well. This cycle was repeated while the necessary adjustments were made to the model based on the objectives stated above. An optimized model satisfying all objectives was obtained after 9 iterations of this procedure. During all molecular mechanics simulations, a distance-dependent dielectric was employed to attenuate the electrostatic terms for H-bond and salt bridge non-bonded interactions. In the final model, the obtained non-bonded interactions were congruent with non-bonded interactions frequently observed in high resolution X-ray structures. We have used this general method successfully, with variations depending on the requirements of the protein/ligand interactions (2,3). A detailed description of quantitative hydropathic interactions can be found in (4).

References

1 Günther S, Reinke PYA, Fernández-García Y, Lieske J, Lane TJ, Ginn HM, Koua FHM, Ehrt C, Ewert W, Oberthuer D, Yefanov O, Meier S, Lorenzen K, Krichel B, Kopicki JD, Gelisio L, Brehm W, Dunkel I, Seychell B, Gieseler H, Norton-Baker B, Escudero-Pérez B, Domaracky M, Saouane S, Tolstikova A, White TA, Hänle A, Groessler M, Fleckenstein H, Trost F, Galchenkova M, Gevorkov Y, Li C, Awel S, Peck A, Barthelmess M, Schlünzen F, Lourdu Xavier P, Werner N, Andaleeb H, Ullah N, Falke S, Srinivasan V, França BA, Schwinzer M, Brognaro H, Rogers C, Melo D, Zaitseva-Doyle JJ, Knoska J, Peña-Murillo GE, Mashhour AR, Hennicke V, Fischer P, Hakanpää J, Meyer J, Gribbon P, Ellinger B, Kuzikov M, Wolf M, Beccari AR, Bourenkov G, von

Stetten D, Pompidor G, Bento I, Panneerselvam S, Karpics I, Schneider TR, Garcia-Alai MM, Niebling S, Günther C, Schmidt C, Schubert R, Han H, Boger J, Monteiro DCF, Zhang L, Sun X, Pletzer-Zelgert J, Wollenhaupt J, Feiler CG, Weiss MS, Schulz EC, Mehrabi P, Karničar K, Usenik A, Loboda J, Tidow H, Chari A, Hilgenfeld R, Uetrecht C, Cox R, Zaliani A, Beck T, Rarey M, Günther S, Turk D, Hinrichs W, Chapman HN, Pearson AR, Betzel C, Meents A. X-ray screening identifies active site and allosteric inhibitors of SARS-CoV-2 main protease. Science. 2021 May 7;372(6542):642-646. Epub 2021 Apr 2. PMID: 33811162; PMCID: PMC8224385.

2 Diaz P, Horne E, Xu C, Hamel E, Wagenbach M, Petrov RR, Uhlenbruck B, Haas B, Hothi P, Wordeman L, Gussio R, Stella N. Modified carbazoles destabilize microtubules and kill glioblastoma multiform cells. Eur J Med Chem. 2018 Nov 5;159:74-89, PMID: 30268825; PMCID: PMC6690746.

3 Burnett JC, Lim C, Peyser BD, Samankumara LP, Kovaliov M, Colombo R, Bulfer SL, LaPorte MG, Hermone AR, McGrath CF, Arkin MR, Gussio R, Huryn DM, Wipf P. A threonine turnstile defines a dynamic amphiphilic binding motif in the AAA ATPase p97 allosteric binding site. Org Biomol Chem. 2017 May 16;15(19):4096-4114, PMID: 28352916; PMCID: PMC5472064.

4 Kellogg GE, Marabotti A, Spyrakis F, Mozzarelli A. HINT, a code for understanding the interaction between biomolecules: a tribute to Donald J. Abraham. Front Mol Biosci. 2023 Jun 7;10:1194962. PMID: 37351551; PMCID: PMC10282649.

Molecular docking to M^{pro}

To determine the feasibility of covalent binding of compounds of interest at the identified Cys300 pocket, these compounds were covalently docked by virtual modeling onto the SARS-CoV-2 main protease crystal structure. Maestro 12.7 (Schrödinger, Inc.) was used to prepare the template M^{pro} crystal structure of PDB:7AXM and the Covalent Docking module was used to model the covalent ligand-protein complex using the Reactive Residue set at Cys300, Reaction Type (Disulfide Formation), and Docking Mode set at Virtual Screening.

Compounds and Reagents

ACV tripeptide, zofenoprilat, epicaptropril, bicisate were from BOC Sciences (Shirely, NY), phosphopantetheine, DL-thiorphan, captopril, R-dihydrolipoic acid and hydrocortisone were from Sigma-Aldrich (St Louis, MO), omapatrilat, emerimide were from Cayman Chemicals (Ann Arbor, MI), tixocortol, and tixocortol pivalate were from Medical Isotopes Inc. (Pelham, NH) and bucilliamine was from AK Scientific (Union City, CA) Nirmatrelvir (NM) was from Med Chem Express (Monmouth Junction, NJ) . All compounds were dissolved in 100% cell culture-grade DMSO from Sigma (St Louis, MO) and stored as 10-20 mM stock solutions at -20^{0}C until use. TKB-198, 5H, and GRL-0920 were obtained as described previously [1-3] and stored as stocks in 100% DMSO. Ammonium hydrogen carbonate for use in SEC/MS chromatography was obtained from Millipore (Oakville, Ontario, CA). Formic acid and trifluoroacetic acid were from Pierce Chemical company (Rockford, IL). Tris(2-carboxyethyl) phosphine hydrochloride (TCEP) solution, dithiothreitol (DTT), and reduced glutathione (GSH) were from Sigma. Sequencing grade chymotrypsin and AccuMAP Low pH Digestion kit was from Promega (Madison, WI). The disulfide of TX was generated by incubation of TX at 1 mM in HEPES buffer pH 7.8 and 10% DMSO overnight at 35^{0}C. The resultant precipitate was dissolved in 100% DMSO and then run on RP-HPLC to purify TSST from remaining TX using a Vydac C18 column and a 2% ACN gradient.

Screening assay for M^{pro} inhibitory activity and determination of M^{pro} covalent modification.

For the screening procedure, M^{pro} activity was measured using a peptide based (TSAVLQSGFRKM) HPLC assay using 100 nM M^{pro} and 50 µM of each drug (see Table S1). Drugs were incubated for 1 h then the assay was started with addition of peptide substrate and stopped after 10 minutes. Products were determined by measuring their absorbance at 205. Control was 5% DMSO and all samples contained 5% DMSO in assay. Further assays involving kinetics and further characterization were performed the same except 50 nM M^{pro} was used in these assays. For assessing covalent modification, each compound (50 µM in DMSO 100%) was incubated with M^{pro} (5 µM) for 1 h in assay buffer (50 mM HEPES buffer, 1 mM EDTA,

50 mM NaCl pH 7.8) and then analyzed by SEC/MS for covalent modification by protein deconvolution. SEC/MS of M^{pro} was carried out using a BioSep SEC2000 column (300 mm × 4.6 mm; Phenomenex, Torrance, CA, U.S.A.) 25 mM ammonium carbonate running buffer made fresh daily (pH adjusted to 7.5 with formic acid). Samples were run on a 1200 series HPLC–MS system (Agilent, Santa Clara, CA, U.S.A.). M^{pro} samples (1 µM-10 µM as indicated in Figures) were injected (2-10 µl) and run with an isocratic flow rate of 0.35 ml · min^{-1} and. Where indicated, cmBSA was sometimes used as an internal standard and carrier to help prevent nonspecific binding of protein during the analysis. M^{pro} eluting from the column was monitored using an Agilent DAD UV detector followed by a FLD detector in series with the Agilent 6230 MS-TOF detector. After different treatments and preincubation times of M^{pro} with test compounds, the eluting M^{pro} peaks detected by the ion current from MS analysis were deconvoluted using Mass Hunter software to assess the molecular mass of M^{pro} and to obtain evidence of covalent modification of the eluting M^{pro} as described previously [4].

Main Protease Kinetic Analysis

Wild type and C300S main proteases were prepared and purified as described previously [4]. To perform Michaelis-Menten kinetics the assay was done in 96 well cell culture treated round bottom plates (Corning). The enzyme was made up as a 60 nM stock in HEPES assay buffer. Eight wells received 38 µl of enzyme solution and each well was then treated with 2 µl of DMSO for controls or 2 µl of 20X stock of TX dissolved in DMSO to bring to 1X. The plate was incubated for 1 h at 37˚C and then 5X substrate stocks in HEPES assay buffer were added to give final substrate concentrations of 0.1, 0.2, 0.4, 0.8, 1.6, 3.2 and 6.4 mM for the DMSO controls and inhibitor treatments. The assay was carried out at 37˚ C for 8 minutes (confirmed to be within the linear range of the assay to obtain initial velocities) and the assay was stopped with 10 µl of 4% TFA solution in water. Samples were assay by RP-HPLC as described above and Lineweaver-Burke (double-reciprocal plots) plots were used to calculate the values of K_M, V_{max}. and K_i. The data presented represents the average of three independent experiments.

***In cellulo* M^{pro} and SARS-Cov-2 antiviral assays:**

Active M^{pro} was expressed from the pcDNA3 H2B-mIFP T2A M^{pro} (WT) plasmid (Addgene 163079). The NanoLuc plasmid containing the M^{pro} cleavage site (AVLQSGFR) was constructed as reported by Chen et al. 2022. Briefly, a permuted NanoLuc construct in the pcDNA3.1 vector expressing amino acids 66-171 in the N-terminus was linked using a linker containing the M^{pro} cleavage site (GGGSGNGSAVLQSGFRSLKACGGG) with amino acids 2-66 of the Nanoluciferase protein in the C-terminus. The NanoLuc construct was codon-optimized for mammalian expression. One hundred thousand early passage healthy cells were plated in each well of a 12-well plate and transfected 24 h later with FUGENE6 (Promega). A ratio of 1:3:3 (NanoLuc:Mpro:Bgal) of plasmid was used for transfection along with pcDNA3 as carrier DNA for maintaining transfection efficiency. Briefly, in each well of the 12-well plate, 80 ng of NanoLuc, 240 ng of Mpro, and 240 ng of the beta-gal control vector were transfected. Inhibitors were added to the cells 20 h post-transfection and assayed for NanoLuc activity 46 h post-inhibitor treatment.

For SARS-CoV-2 replication assays, HeLa-Ace2 cells obtained from Creative Biogene (Shirley, NY) were seeded into 384-well tissue culture treated plates at 6,000 per well in 30 µL DMEM (Gibco, Gaithersburg, MD, USA) supplemented with 10% fetal bovine serum (FBS; Sigma, St. Louis, MO, USA) the day prior to infection. One hor 18 hrs before infection, compounds (dissolved in DMSO) were digitally dispensed directly into cell plates using a Tecan D300e digital dispenser to generate a twelve-point dose curve for each compound, replicated in quadruplicate (n = 4). Under biocontainment conditions, SARS-CoV-2 virus (WA-01) was diluted in DMEM with 10% FBS to a concentration of 3,000 plaque forming units (PFU) per 20 µL (60,000 PFU/mL) (MOI of 2). This inoculum was added to the assay plates for a final assay volume of 50 µL. Plates were fixed in 10% neutral buffered formalin 18 hours post-infection; Upon removal from biocontainment, cells were stained with a SARS-CoV/SARS-CoV-2 nucleoprotein-specific primary antibody followed by secondary antibody conjugated to Alexa647 fluorophore. Hoechst dye was added for detection of cell nuclei. Fluorescence readout was quantitated using a PerkinElmer Operetta

high-content imaging system. Cytotoxicity on mock-infected plates was determined using the Promega Cell Titer-Glo Luminescent Cell Viability Assay (Catalog #G7571) at the time of fixation of the infected plate. Half-maximal inhibitory concentration (IC_{50}) and 50% cytotoxic concentration (CC_{50}) were calculated using GraphPad Prism Software (La Jolla, CA). Z' factor scores were assessed as quality-control parameters for each plate.

Determination of TP metabolic fate when added to serum or cells:

To determine if TP is converted to TX under various conditions, we incubated TP (50 µM) in water, DMEM, DMEM supplemented with heat inactivated serum or DMEM with 10% serum that was not heat inactivated. Following an 18 h incubation overnight at 37°C the samples were acidified with 0.2% TFA to stop the reaction and then diluted with DMSO to give a final of 50% DMSO. This was done to ensure solubility of the compounds prior to RP/HPLC/MS analysis. The samples were treated with 10 mM TCEP for 15 min (to reduce and disulfide bound TX or TSST in the samples) and then separated on a VyDac C18 column 5205 and the amount of TP and TX was determined based on the elution time and molecular mass obtained with the standards. To assess the conversion of TP by cells, HeLa cells were plated overnight and then cells were treated with TP (50 µM). Cells were then extracted for metabolites after 1, 4, 24, and 48 hincubation. Cells were washedwith PBS the cells were then trypsinized followed by three washes with PBS. The pellet was then extracted with 60% methanol solution/0.2% TFA and heated at 95 degrees for 5 minutes. Cellular debris was removed by centrifugation and the methanolic/TFA solution dried by speed vac to dryness. The residue was dissolved in 100% DMSO and analyzed by RP-HPLC/MS. Shown are the levels of TP, TX, TSSG and the disulfide of TX.

Purification of tixocortol disulfide (TSST).

To purify tixocortol disulfide for use in M^{pro} assays, TX was first incubated in HEPES assay buffer pH 7.8 in 5% DMSO. The reaction was left to go overnight at 37°C. TSST precipitated from the buffer and was pelleted and then redissolved in 100% DMSO. The solution was then separated on a VyDac C18 column 5205 and the eluting TSST as identified by its mass obtained from MS analysis was collected in eppendorph tubes. The eluates were then dried down in a speed Vac concentrator, incubated with methanol to remove volatiles and dried again. The powder was redissolved in 100% DMSO. The TSST could be converted to TX with 10 mM TCEP and then the concentration determined by comparison to a known concentration of YTX standard. The TSST in DMSO was stored at -70°C until use.

Preparation of M^{pro} TX for chymotryptic digestion and RP-HPLC/MS analysis.

To determine which cysteines of M^{pro} were modified by tixocortol treatment, we first prepared TX- modified M^{pro} (TX-M^{pro}). M^{pro} was first pretreated with 10 mM TCEP to ensure full reduction of the 12 cysteines and the correct native mass was verified by SEC/MS analysis as described above. The TCEP was removed by washing through an Amicon 10 kDa cutoff membrane three times using 50 mM HEPES buffer pH 7.8 with 1 mM EDTA, 10% DMSO and 50 mM NaCl. Protease was set at 1 µM and TX was added at a final concertation of 200 µM and incubated at 35°C for 1 h (total volume 3.5 ml). The preparation was then concentrated using a 10 kDa membrane and washed three times with HEPES buffer pH 7.2 with 1 mM EDTA, 10% DMSO to remove the residual unbound TX. The TX-M^{pro} preparation was analyzed by SEC/MS to determine the extent of TX modification. To determine which cysteines were modified by TX, we carried out chymotryptic digestions as described previously using the AccuMAP Low pH Digestion kit from Promega [4]. Briefly, 20 µg of TX-M^{pro} was alkylated with NEM in 8 M urea, concentrated by filtration, and put up in final 1 M urea pH 8 in Tris and CaCl2 buffer. The alkylated preparation in 1 M urea was digested with chymotrypsin (1 µg/ml in 1 mM HCl) at 28°C overnight. The solution was stopped with a final of 2% TFA. The samples were then applied to C18 spin columns and after washing, the peptides were eluted with acetonitrile. Peptide samples were put up into RP-HPLC running buffer (0.1% FA/0.02% TFA).

The peptide samples, treated without or with 10 mM TCEP as well as the corresponding peptide standards and TX-modified peptide standards were analyzed by RP-HPLC/MS as described previously [4].

1. N. Higashi-Kuwata, K. Tsuji, H. Hayashi, H. Bulut, M. Kiso, M. Imai, H. Ogata-Aoki, T. Ishii, T. Kobayakawa, K. Nakano, N. Takamune, N. Kishimoto, S. I. Hattori, D. Das, Y. Uemura, Y. Shimizu, M. Aoki, K. Hasegawa, S. Suzuki, A. Nishiyama, J. Saruwatari, Y. Shimizu, Y. Sukenaga, Y. Takamatsu, K. Tsuchiya, K. Maeda, K. Yoshimura, S. Iida, S. Ozono, T. Suzuki, T. Okamura, S. Misumi, Y. Kawaoka, H. Tamamura and H. Mitsuya, Identification of SARS-CoV-2 M(pro) inhibitors containing P1' 4-fluorobenzothiazole moiety highly active against SARS-CoV-2, *Nat Commun*, 2023, **14**, 1076.
2. K. Tsuji, T. Ishii, T. Kobayakawa, N. Higashi-Kuwata, C. Azuma, M. Nakayama, T. Onishi, H. Nakano, N. Wada, M. Hori, K. Shinohara, Y. Miura, T. Kawada, H. Hayashi, S. I. Hattori, H. Bulut, D. Das, N. Takamune, N. Kishimoto, J. Saruwatari, T. Okamura, K. Nakano, S. Misumi, H. Mitsuya and H. Tamamura, Potent and biostable inhibitors of the main protease of SARS-CoV-2, *iScience*, 2022, **25**, 105365.
3. S. I. Hattori, N. Higashi-Kuwata, H. Hayashi, S. R. Allu, J. Raghavaiah, H. Bulut, D. Das, B. J. Anson, E. K. Lendy, Y. Takamatsu, N. Takamune, N. Kishimoto, K. Murayama, K. Hasegawa, M. Li, D. A. Davis, E. N. Kodama, R. Yarchoan, A. Wlodawer, S. Misumi, A. D. Mesecar, A. K. Ghosh and H. Mitsuya, A small molecule compound with an indole moiety inhibits the main protease of SARS-CoV-2 and blocks virus replication, *Nat Commun*, 2021, **12**, 668.
4. D. A. Davis, H. Bulut, P. Shrestha, A. Yaparla, H. K. Jaeger, S. I. Hattori, P. T. Wingfield, J. J. Mieyal, H. Mitsuya and R. Yarchoan, Regulation of the Dimerization and Activity of SARS-CoV-2 Main Protease through Reversible Glutathionylation of Cysteine 300, *mBio*, 2021, **12**, e0209421.